DLI-CVD of TiO_2–Cu antibacterial thin films: Growth and characterization

J. Mungkalasiri [a,b], L. Bedel [b], F. Emieux [b], J. Doré [c], F.N.R. Renaud [c], F. Maury [a,*]

[a] CIRIMAT, CNRS/INPT/UPS, ENSIACET, 118 Route de Narbonne, 31077 Toulouse cedex 4, France
[b] LTS/DTNM, CEA Grenoble, 17 rue des martyrs, 38054 Grenoble, France
[c] Nosoco.Tech®, Université Lyon 1, EA 3090, Lyon, France

A B S T R A C T

TiO_2–Cu nanocomposite films were grown by pulsed direct liquid injection chemical vapor deposition (DLI-CVD) on stainless steel, silicon and glass substrates with the goal to produce bactericidal surfaces. Copper bis (2,2,6,6-tetramethyl-3,5-heptadionate), $Cu(TMHD)_2$, and titanium tetra-*iso*-propoxide, TTIP, were used as metalorganic precursors. Liquid solutions of these compounds in xylene were injected in a flash vaporization chamber connected to a cold wall MOCVD reactor. The deposition temperature was typically 683 K and the total pressure was 800 Pa. The copper content of the layers was controlled by the mole fraction of Cu $(TMHD)_2$ which was adjusted by the injection parameters (injection frequency and concentration of the starting solution). The chemical, structural and physical characteristics of the films were investigated by XRD, XPS, FEG-SEM and TEM. Copper is incorporated as metal particles with a relatively large size distribution ranging from 20 to 400 nm (with a large majority in 20–100 nm) depending on the copper content of the films. The influence of the growth conditions on the structural features and the antibacterial properties of the thin films are reported and discussed.

Keywords:
DLI-CVD
Copper
Titanium dioxide
Nanocomposite coatings
Antibacterial surfaces

1. Introduction

Bacteria essentially exist and multiply in biofilms that grow on various surfaces. They cause significant problems of infection that spread in many areas. Today great efforts attempt to prevent the formation of biofilms. The post treatments of contaminated surfaces as chemical or physical cleanings do not settle the problem because they are curative and not preventive solutions. Long term antibacterial surfaces are required. Many solutions were proposed in the literature using high-technology surface treatments and growth of antibacterial thin films. For instance, works were reported on the ion implantation of copper or silver [1,2], on the deposition of SiO_2–Ag [3], TiO_2 [4], TiN–Cu [5], and other thin films containing triclosan [6] or quaternary ammonium salt [7] as well as on glasses and alloys doped with antibacterial elements [8].

Anatase TiO_2 under UV radiation is a well known photocatalytic material [9]. The self cleaning property by decomposition of organic species and antibacterial activity were previously reported [4,10]. This antibacterial coating is very efficient but UV light is necessary and for many applications the use of UV is not possible or could be dangerous. Furthermore, it is not an economic solution since electrical energy is required for UV lamps [11].

The addition of metals (Cu, Ag, Au, Co, Fe, etc.) to TiO_2 was carried out to improve the photocatalytic activity [12–14]. For instance, it was found that a suitable amount of silver (2–4 mol%) increased the photocatalytic activity of TiO_2 films grown by sol–gel [15]. Many other deposition processes have also been used for the growth of doped-TiO_2 as CVD and PVD films. The antibacterial properties of copper have been known for centuries. Its efficiency was discussed in many papers [8,16]. Several possible mechanisms of copper activity on bacteria have been discussed. Copper ions exhibit a high affinity for the thiol and amino groups present in proteins. Thus, specialized proteins containing clusters of these functional groups transport and store the copper ions, hampering their potential toxicity [17].

The direct liquid injection chemical vapor deposition process (DLI-CVD) presents advantages for large scale surface treatment such as a high growth rate, a good control of the chemical composition of the films, the deposition under atmospheric or moderately reduced pressure as well as the possibility to coat complex and porous substrates. We have recently used this process for the growth of TiO_2–Ag films and the results will be published soon. In this paper, TiO_2–Cu nanocomposite films were deposited in one-step by DLI-CVD for antibacterial applications. The influence of the growth conditions on the main structural features of the films is presented. The antibacterial properties were found to increase with the copper content of these nanocomposite coatings.

2. Experimental

2.1. Film preparation

The TiO_2–Cu thin films were deposited in a vertical cold wall CVD reactor equipped with a pulsed Direct Liquid Injection system (Fig. 1).

* Corresponding author. Tel.: +33 562885669; fax: +33 562885600.
E-mail address: francis.maury@ensiacet.fr (F. Maury).

Liquid solutions of the precursors were introduced through injectors at the top of a flash vaporization chamber and then reactive vapors were carried down to the deposition zone under low pressure using a carrier gas (N_2). Before reaching the substrates, the vapor passed through a showerhead which distributed the precursors homogeneously on the sample holder. A vacuum pump was used to eliminate the gaseous by-products including the carrier gas and solvent. The total pressure was controlled independently of both the atmosphere and the total flow rate using an automatic system. It was maintained constant at 800 Pa.

The substrates (stainless steel 316 L, Si and glass) were cleaned with acetone (15 min in an ultrasonic bath) prior to use and then rinsed with ethanol before being dried by air stream. The TiO_2–Cu films were grown using two metalorganic precursors as Cu and Ti sources that we have previously employed in conventional MOCVD: copper bis(2,2,6,6-tetramethyl-3,5-heptadionate) ($Cu(TMHD)_2$) [18] and titanium tetra-*iso*-propoxide (TTIP) [9]. Here they were dissolved in xylene as solvent. Pure N_2 (99.9999%) and O_2 (99.9999%) were used as carrier gases (N_2:O_2 = 9:1). The gas flow rates were monitored by mass flow controllers. The mole fractions of $Cu(TMHD)_2$ and TTIP were controlled by the injection parameters (Table 1). Two injectors were used to feed the reactor: one for the Ti source and the other for Cu. The evaporator and the showerhead were maintained at 473 K. The reactor wall was heated at 540 K to avoid the condensation of the reagents. The deposition temperature was fixed at 683 K except otherwise specified for a series of experiments. The film thickness was controlled by varying the deposition time. The mole fraction of the copper precursor in the input gas phase is the main parameter that controls the Cu content of the films. It was varied either by adjusting the solution concentration or the injection frequency while the other parameters were maintained constant as reported in Table 1. We will focus on the influence of the mole fractions of $Cu(TMHD)_2$.

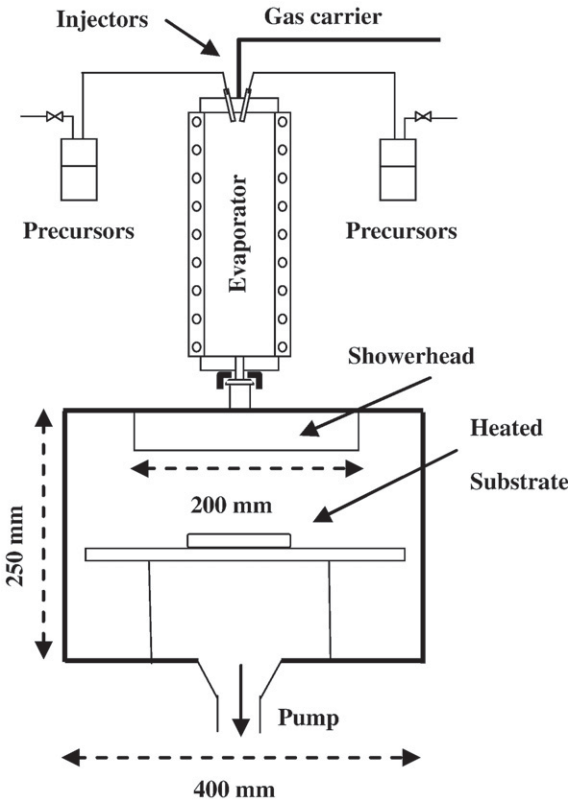

Fig. 1. Sketch of the DLI-MOCVD reactor.

Table 1
Experimental DLI-CVD conditions for the growth of TiO_2–Cu nanocomposite films.

Deposition temperature (K)	623–723
Total pressure (Pa)	800
N_2 carrier gas (sccm)	324
O_2 carrier gas (sccm)	36
TTIP concentration in xylene (mol L^{-1})	1
TTIP injection frequency (Hz)	2
TTIP injection opening time (ms)	2
$Cu(TMHD)_2$ concentration in xylene (mol L^{-1})	0.005–0.1
$Cu(TMHD)_2$ injection frequency (Hz)	0.5–4
$Cu(TMHD)_2$ injection opening time (ms)	2

The mole fraction of the Cu precursor was the main parameter varied either by adjusting the solution concentration or the injection frequency.

2.2. Film characterization

The films grown on Si wafers were used to analyze the composition and the microstructure. The structure was determined by X-ray diffraction (XRD) using a θ–2θ or grazing angle configuration. The morphology and film thickness were investigated with a scanning electron microscope (Leo 1530 FEG-SEM) equipped with an X-ray energy dispersive spectroscopy analyzer (EDX). The size of Cu particles was measured by transmission electron microscopy (TEM). The film composition was analyzed by X-ray photoelectron spectroscopy (XPS). The JIS Z 2801 standard with *Staphylococcus aureus* was applied as antibacterial test on samples generally prepared on glass. More details on this bacteriological standard test will be reported in a future paper.

3. Results and discussion

3.1. Film morphology

A granular surface morphology is observed for pure TiO_2 DLI-CVD films both on Si and stainless steel substrates. It is constituted of small lamellar grains of 50–100 nm width that agglomerate to form bigger nodular grains (200–300 nm in diameter) leading to a relatively high surface roughness (Fig. 2a). The TiO_2–Cu nanocomposite films still exhibit a granular morphology but the grains are smaller and less agglomerated. It seems to be more compact. The surface is smoother (Fig. 2b). The copper particles are uniformly distributed in the TiO_2 matrix with particle sizes in the range of 50 to 250 nm as observed by SEM. The largest Cu particles emerge from the surface of the thinnest layers (Fig. 2c). The number of Cu particles visible on the surface seems to increase with the $Cu(TMHD)_2$ mole fraction. By reducing the deposition temperature from 683 to 623 K, the nanocomposite films exhibit a denser structure due to the quasi amorphous structure of the oxide matrix (Fig. 2d). No significant influence of the substrate was found on the morphology of these nanocomposite layers.

3.2. Growth rate

The deposition rate of pure TiO_2 films is high (115 nm min^{-1}). It decreases quickly to approximately 60 nm min^{-1} when the $Cu(TMHD)_2$ mole fraction is increased and reaches a nearly constant level already at a $Cu(TMHD)_2$ mole fraction of 0.15% (Fig. 3). This behavior could be due to premature interactions between the two precursors in the gas phase or in the showerhead but no evidence for that was observed at 683 K. So it can be assumed that (i) a competition occurs on the adsorption sites for the two molecular precursors and (ii) the nucleation and growth of Cu particles hinder the growth of TiO_2 crystals that form the matrix. It is frequently observed in CVD that doping influences the kinetics of the process.

For a series of experiments the deposition temperature was increased from 623 to 723 K and the growth rate of TiO_2–Cu was found to

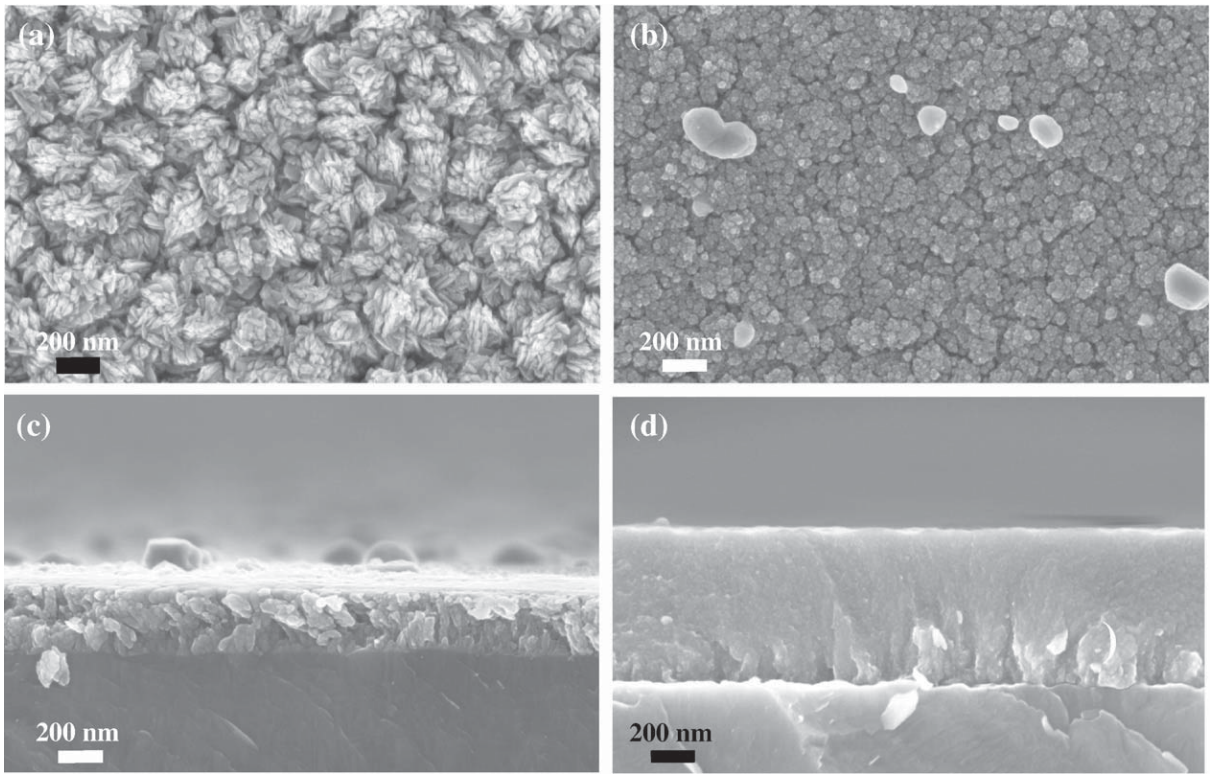

Fig. 2. FEG-SEM micrographs of TiO_2–Cu films deposited on silicon wafer as a function of the $Cu(TMHD)_2$ mole fraction in the reactive gas phase: (a) 0% at 683 K (pure TiO_2); (b) 0.076% at 683 K (surface morphology); (c) 0.076% at 683 K (cross section); (d) 0.076% at 623 K (cross section). The scale bar is the same for each micrograph.

decrease from 40 to 18 nm min^{-1} (Fig. 4). This contrasts with the deposition by low pressure MOCVD of pure TiO_2 which was found to be thermally activated [19]. The vapor of solvent (xylene) in this DLI-CVD process probably plays a role on the kinetics but further research work is need to support this hypothesis. On the other hand, by increasing the deposition temperature, premature reactions can occur in the gas phase which consumes reagents. For instance, Fig. 4 also shows that the relative content of copper in the films decreases by increasing the growth temperature, as deduced from the Cu/Ti EDX ratio intensities, indicating a preferential decomposition of the Cu precursor before reaching the deposition zone. This is consistent with the fact that this precursor is the less thermally stable [18]. At this stage, we have not tried to optimize the growth rate or to study the deposition mechanisms. Further experiments are required for such a discussion, in particular because of the great complexity of the reactive gas phase (TTIP/Cu $(TMHD)_2/N_2/O_2$). We have also to consider that the growth rate of anatase is generally faster than that of rutile and we will see in the next section that both phases can be formed depending on the growth conditions.

3.3. Structure, microstructure and composition of the films

The XRD pattern of a TiO_2–Cu coating grown at 683 K (300 nm thick) reveals that the TiO_2 matrix crystallizes with the anatase structure and copper is present in the metallic form (Fig. 5). No evidence for copper oxide was found by XRD. This was supported by XPS analysis. The binding energies of Ti $2p_{3/2}$ and O 1s found at 458.9 eV and 530.1 eV, respectively, are in good agreement with TiO_2. The absence of shake-up satellites between Cu $2p_{3/2}$ and Cu $2p_{1/2}$ and the binding energy of Cu $2p_{3/2}$ found at 932.5 eV indicate the absence of CuO. This is confirmed by comparison with a recent work where CuO was deposited with TiO_2 [20]. The presence of Cu_2O is more

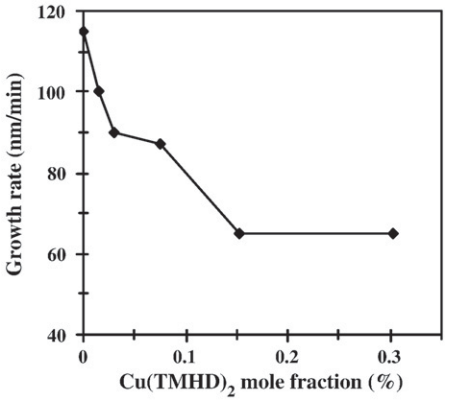

Fig. 3. Influence of the $Cu(TMHD)_2$ mole fraction on the growth rate of TiO_2–Cu films ($T = 683$ K).

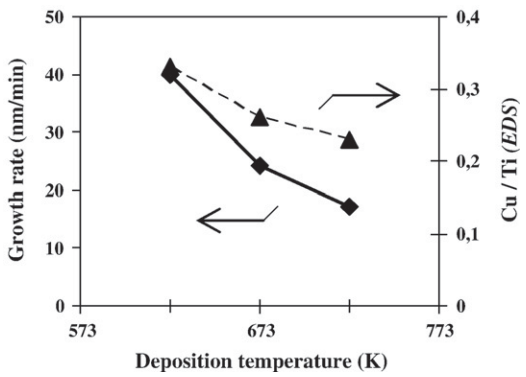

Fig. 4. Influence of the growth temperature on the deposition rate and on the content of copper in TiO_2–Cu films (EDX analyses).

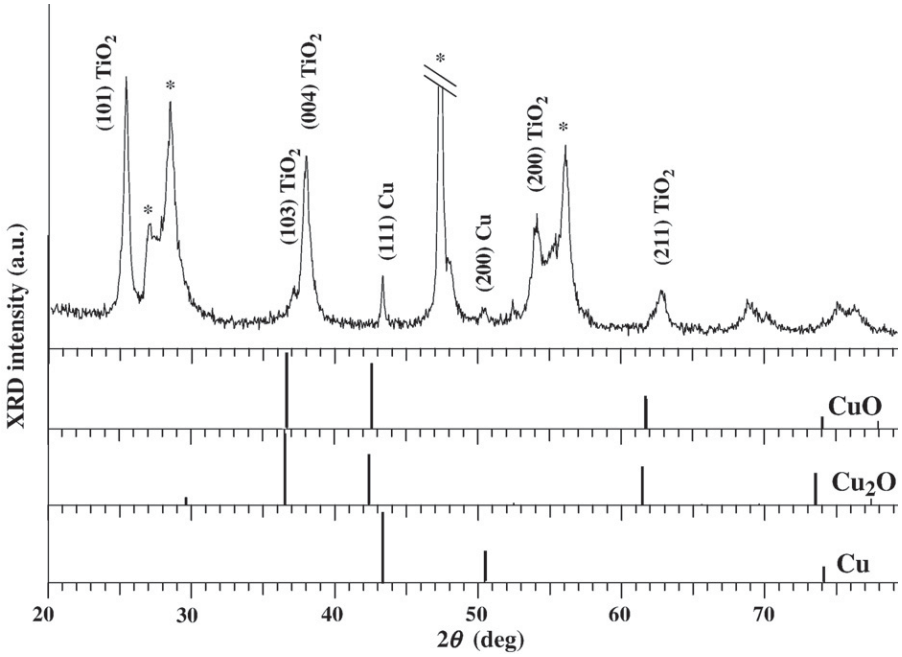

Fig. 5. Grazing angle XRD pattern of a TiO_2–Cu film showing the presence of anatase and metallic copper. Peaks noted with an asterisk originate from the substrate.

difficult to detect and this is generally achieved from the Auger parameter (A.P. is defined as the difference between the kinetic energy of the Auger and XPS electrons). Such analysis reveals that Cu_2O exists on the surface of our as-deposited samples (typically A.P. = 1849.7 eV) but tends to disappear after Ar^+ sputtering for a few minutes to clean the surface contamination. This indicates that only the Cu metal particles emerging from the surface of the film are superficially oxidized due to interaction with the air.

The presence of metal Cu particles (and not of Cu_2O) was definitively demonstrated by TEM (Fig. 6). The lattice parameter measured for the metallic particles at 0.3615 nm is in good agreement with the cubic fcc structure of metal Cu and far from that of Cu_2O (0.4245 nm).

The influence of the $Cu(TMHD)_2$ mole fraction in the input gas phase on the film composition is given in Fig. 7. Both XPS and XRD analyses confirm an increase of the Cu content of the films with the $Cu(TMHD)_2$ mole fraction. This indicates that the film activity which is certainly related to the Cu content could be controlled only by this growth parameter.

Interestingly, the formation of rutile was observed by XRD when the Cu content increased in the films while the deposition temperature was maintained constant at 683 K (Fig. 8). The correlation between the increase of rutile with Cu content suggests that this metal favors the crystallization of rutile. This was reported for other metals as for TiO_2–Ag deposited by sol–gel [15].

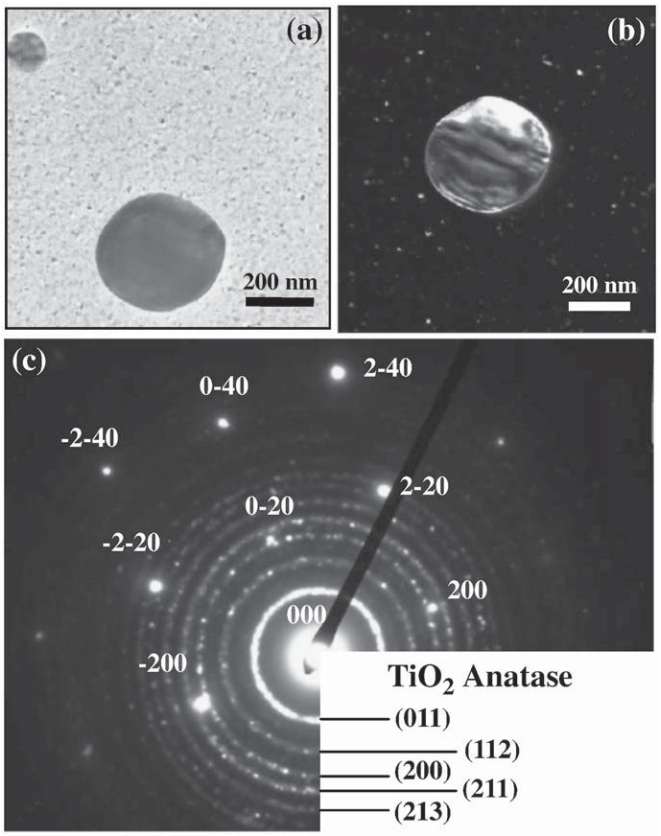

Fig. 6. TEM analyses of a TiO_2–Cu film: (a) bright field image of one of the biggest Cu particles; (b) dark field image; (c) corresponding selected area electron diffraction pattern.

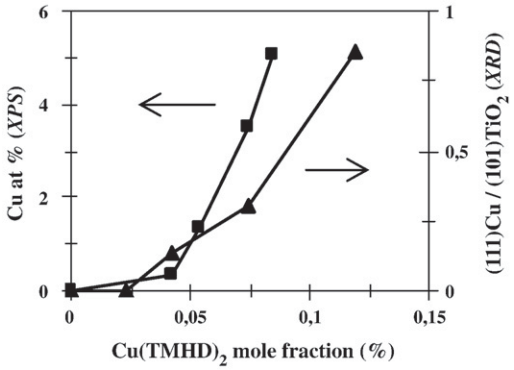

Fig. 7. Variation of the Cu content in the films determined by XPS (at.%, left axis) and ratio of (111) Cu/(101) TiO_2 XRD intensity (right axis, θ–2θ configuration) as a function of the $Cu(TMHD)_2$ mole fraction in the input gas phase.

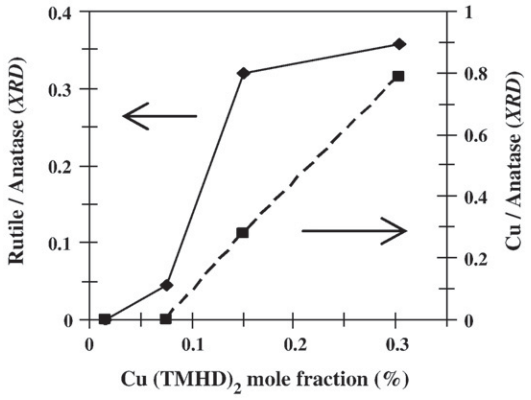

Fig. 8. Influence of the $Cu(TMHD)_2$ mole fraction in the input gas phase on the relative content of rutile and copper as determined from XRD intensity ratios (110)Rutile/(101) Anatase and (111)Cu/(101)Anatase.

It is well known that the smaller the crystallites, the broader the XRD peaks. So the average crystallite size (t) can be derived from the broadening of the diffraction peaks using the Scherrer equation:

$$t = K\lambda / (B\cos\theta) \quad (1)$$

where K is a dimensionless shape factor (0.9), λ is the wavelength of the X-rays and B is the integral breadth of a reflection (in radians 2θ) located at the Bragg angle 2θ. B is often calculated from the line broadening at half maximum intensity (FWHM) relative to a reference solid with crystallite size >500 nm according to $B^2 = B_s^2 - B_r^2$.

The average crystal size of TiO_2 determined from the (101) TiO_2 XRD peak increases with the film thickness to reach typically 40 nm for a 100 nm thick layer. We noted that an increase of the $Cu(TMHD)_2$ mole fraction decreased the growth rate of the films and we also observed that it decreases the mean crystal size of anatase and rutile. This confirms that the deposition of Cu particles hinders the growth of TiO_2 crystals.

TEM analyses have revealed a uniform distribution of the Cu particles both on the surface and through the layer thickness. No agglomeration of Cu particles was found and different particle sizes with a spherical shape ranging from 20 to 400 nm were observed (with a large majority in the range of 20–100 nm). Fig. 9 shows the size distribution of Cu particles in the nanocomposite film. These particle sizes are in good agreement with the values determined by FEG-SEM. A detailed analysis of the TEM images indicates that the population density of small (20–100 nm) Cu particles (10^8 particles cm^{-2}) is significantly higher than the largest ones. These largest Cu particles are typically in the ranges of 100–250 nm and >250 nm as deduced from different samples. It is possible that Cu particles smaller than 20 nm are present but they are not detected by our TEM analyses.

3.4. Antibacterial activity

Antibacterial activity was the motivation of this work and copper was selected as bactericidal agent with the goal to use a minimum amount in the films. The mole fraction of $Cu(TMHD)_2$ was varied since it allows to control the Cu content of the films. According to the JIS Z 2801 standard the antibacterial activity was calculated by the following formula:

$$Antibacterial\,activity = \mathrm{Log}\,(A / B) \quad (2)$$

where A and B are the number of CFU (colony forming unit) on the surface of the reference and treated samples, respectively. For convenient comparisons between various series, we use also a definition of the relative activity given by:

$$Relative\,activity = [\mathrm{Log}\,(A / B) / \mathrm{Log}\,(A)]{*}100. \quad (3)$$

This relative activity means that when it is equal to 100% the surface is bactericidal, in the range of 0–100% the surface has an antibacterial behavior and zero means the surface is inactive.

Fig. 10 shows that an antibacterial activity is detected for mole fractions of $Cu(TMHD)_2$ higher than 0.05% and a bactericidal efficiency

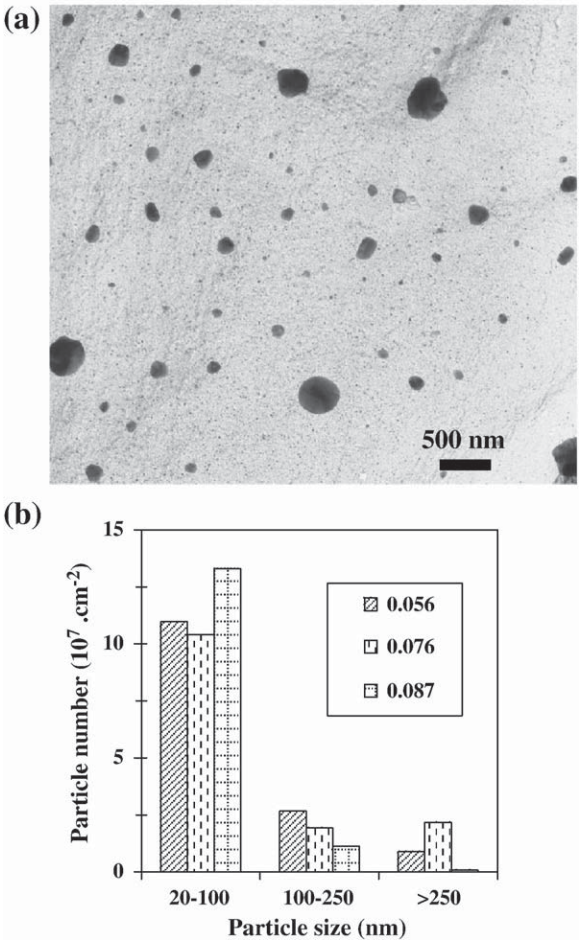

Fig. 9. TEM micrograph of a TiO_2–Cu film deposited at 683 K directly on a microscopy grid made of amorphous carbon (a) and size distribution of the density of particles for different mole fractions of $Cu(TMHD)_2$ in the gas phase (b): 0.056%, 0.076% and 0.087%.

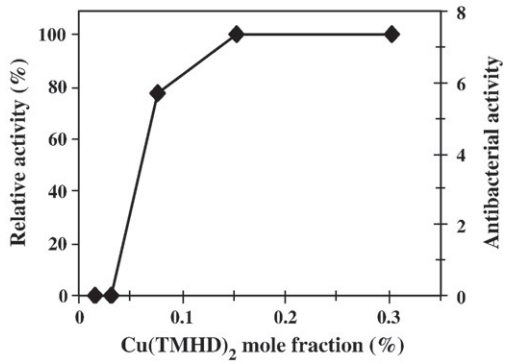

Fig. 10. Influence of the $Cu(TMHD)_2$ mole fraction in the input gas phase on the antibacterial activity with *Staphylococcus aureus* of TiO_2–Cu films. Results are presented as standard antibacterial activity according to the JIS Z 2801 standard (right axis; Eq. (2) in the text) and as relative antibacterial activity (left axis; Eq. (3) in the text).

is observed for mole fractions higher than 0.15%. This means that the number of bacteria reduced from 10^7 colonies/mL to 0 colony in 24 h under standard conditions, *i.e.* without UV irradiation.

Specific experiments to analyze the long term stability of these bactericidal surfaces are currently in progress. At this stage, we have observed a slight decrease of the biocidal property after 5 months of storage under various conditions since samples that exhibited a bactericidal behavior (100% of relative activity) reveal a relative antibacterial activity of approximately 70%. More details will be discussed elsewhere.

4. Conclusions

TiO_2–Cu nanocomposite films were deposited by DLI-CVD under low pressure (800 Pa) at 683 K on stainless steel, silicon and glass substrates using $Cu(TMHD)_2$ and TTIP as Cu and Ti sources, respectively. N_2 and O_2 were used as carrier and reactive gases, respectively. The mole fraction of the Cu precursor influences the morphology, the structure and the growth rate of the TiO_2–Cu films while the other parameters were maintained constant. At 683 K, TiO_2 crystallizes with the anatase structure but increasing the Cu content of the film favors the rutile nucleation and growth. Cu is incorporated as metallic and spherical particles which are uniformly dispersed on the surface and well distributed through the thickness of the layers. Most of the Cu particle sizes are in the range of 20 to 100 nm. The DLI-MOCVD process is suitable for the growth of multifunctional layers as TiO_2–Cu with a high output. A more thorough investigation of the antibacterial properties of these films will be described in a future paper in relation with the Cu content of the layers since this appears as a key feature.

Acknowledgements

The authors thank Dr. C. Sarantopoulos (CIRMAT, Toulouse) for fruitful discussion on structural characterization and C. Anglade and M. Jouve (CEA, Grenoble) for technical assistance. This work was supported by CEA, CNRS and ANR under contract ANR-06-MAPR-0007-01.

References

[1] Z.G. Dan, H.W. Ni, B.F. Xu, J. Xiong, P.Y. Xiong, Thin Solid Films 492 (2005) 93.
[2] Y.Z. Wan, S. Raman, F. He, Y. Huang, Vacuum 81 (2007) 1114.
[3] H.J. Jeon, S.C. Yi, S.G. Oh, Biomaterials 24 (2003) 4921.
[4] P. Evans, D.W. Sheel, Surf. Coat. Technol. 201 (2007) 9319.
[5] X.B. Tian, Z.M. Wang, S.Q. Yang, Z.J. Luo, R.K.Y. Fu, P.K. Chu, Surf. Coat. Technol. 201 (2007) 8606.
[6] W. Zhang, P.K. Chu, J. Ji, Y. Zhang, R.K.Y. Fu, Q. Yan, Polymer 47 (2006) 931.
[7] M. Marini, M. Bondi, R. Iseppi, M. Toselli, F. Pilati, Eur. Polym. J. 43 (2007) 3621.
[8] J.O. Noyce, H. Michels, C.W. Keevil, J. Hosp. Infect. 63 (2006) 289.
[9] F.-D. Duminica, F. Maury, R. Hausbrand, Surf. Coat. Technol. 201 (2007) 9304.
[10] A.G. Rincon, C. Pulgarin, Appl. Catal. B Environ. 49 (2004) 99.
[11] N. Lu, Z. Zhu, X. Zhao, R. Tao, X. Yang, Z. Gao, Biochem. Biophys. Res. Commun. 370 (2008) 675.
[12] W. Zhang, Y. Chen, S. Yu, S. Chen, Y. Yin, Thin Solid Films 516 (2008) 4690.
[13] I.M. Arabatzis, T. Stergiopoulos, M.C. Bernard, D. Labou, S.G. Neophytides, P. Falaras, Appl. Catal. B Environ. 42 (2003) 187.
[14] L. Bugyi, A. Berko, L. Ovari, A.M. Kiss, J. Kiss, Surf. Sci. 602 (2008) 1650.
[15] C. He, Y. Yu, X. Hu, A. Larbot, Appl. Surf. Sci. 200 (2002) 239.
[16] M. Joseph, M. Kuriakose, M.R.P. Kurup, E. Suresh, A. Kishore, S.G. Bhat, Polyhedron 25 (2006) 61.
[17] M.E. Letelier, A.M. Lepe, M. Faundez, J. Salazar, R. Marin, P. Aracena, H. Speisky, Chem.-Biol. Interact. 151 (2005) 71.
[18] F. Maury, S. Vidal, A. Gleizes, Adv. Mater. Opt. Electron. 10 (2000) 123.
[19] C. Sarantopoulos, A.N. Gleizes, F. Maury, Surf. Coat. Technol. 201 (2007) 9354.
[20] H.M. Yates, L.A. Brook, I.B. Ditta, P. Evans, H.A. Foster, D.W. Sheel, A. Steele, J. Photochem. Photobio. A: Chem. 197 (2008) 197.